Probing Molecular Assembly of Small Organic Molecules During Meniscus Guided Coating Using Experimental and Molecular Dynamics Approaches

Stephanie Guthrie[1, ‡], Yuan Gao[2, ‡], Kevin Stone[3], Baoxing Xu[2,*], Gaurav Giri[1,*]

[1]Department of Chemical Engineering, University of Virginia, Charlottesville, Virginia, 22904, United States
[2]Department of Mechanical and Aerospace Engineering, University of Virginia, Charlottesville, Virginia, 22904, United States
[3]Stanford Synchrotron Radiation Lightsource, SLAC National Accelerator Laboratory, Menlo Park, CA, 94025, USA
‡Equal Contribution
*Corresponding Authors: Gaurav Giri, gg3qd@virginia.edu and Baoxing Xu, bx4c@virginia.edu

ABSTRACT

Evaporation based thin film coating processes are ubiquitous in fields such as organic electronics, dye coatings, and the pharmaceutical industry. Based on experimental observations of enhanced thin film alignment during meniscus guided coating (MGC), a molecular dynamics simulation was developed to describe the thin film formation that occurs due to the interplay of evaporation and fluid dynamics. The process of solvent evaporation from solution is first examined, which leads to the formation of a solid thin film after evaporation is complete. Next, a MGC process was simulated by introducing a flow profile to the evaporative system. Through this, we gain insight to how molecules respond and reorient in the presence of a flow profile. These results indicate that both the evaporation and the flow profile have a hand in orienting small molecules in a thin film during the MCG process. Combining experimental techniques with simulations help enhance understanding of the forces that are significant in molecular aggregation during coating processes.

TABLE OF CONTENTS GRAPHIC

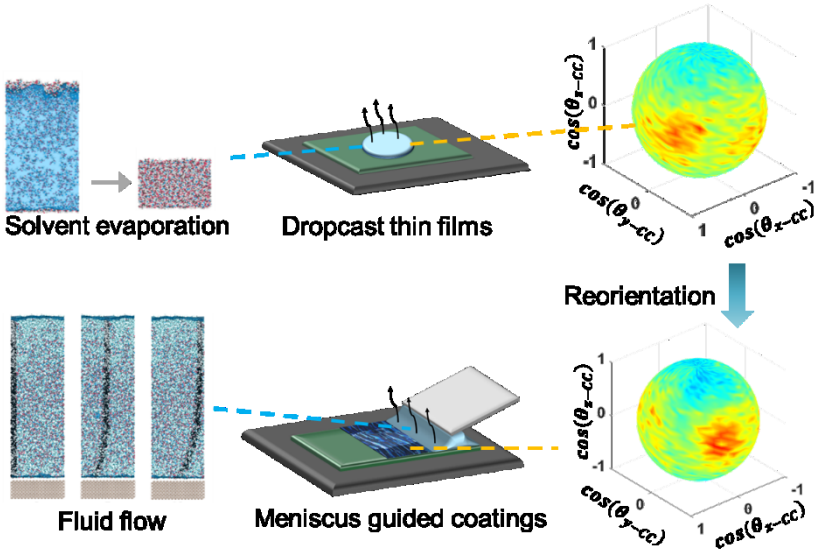

INTRODUCTION

Crystallization is an important processing step that is utilized in multiple fields, including pharmaceutical, food, and organic electronics industries.[1–3] Crystallization is dependent on molecular assembly and molecular densification, which precede crystal nucleation and growth.[4] Many innovative and novel techniques for solution mediated crystallization have been developed to control crystal polymorph, morphology, and habit. Some of these technologies include antisolvent and supercritical CO_2 based crystallization, spray drying, inkjet printing, microfluidic crystallization, and meniscus guided coating (MGC).[5–8] MGC processes are particularly promising and have gained attention for solid thin film formation of small molecules and polymers, due to the ease of scaling up the process and the ability to create thin films with uniform morphology.[8,9]

MGC techniques have been used to create thin films of polymers and organic semiconductors for organic photovoltaics, organic electronics and optoelectronics, and pharmaceutical applications.[8–11] For example, MGC has facilitated control over crystal structure and morphology in organic semiconductors, where device performance is dependent on the formation of single crystal domains to achieve high charge transport.[12] Demonstrating precise control over crystal properties is also relevant in oral thin film pharmaceutical formulations, where active material needs to dissolve and become active on a rapid timescale.[13] Guthrie et al. described the thin film morphology, crystallization behavior, and polymorphism of glycine and acetaminophen using MGC.[8] For glycine, metastable (α and β) polymorphs were reproducibly isolated as a function of thin film coating parameters and film thickness. Horstman et al. performed a similar study using aspirin and ellipticine as the molecules of interest, and also noted the ability to control crystal morphology and polymorphism as a function of processing parameters.[9]

It is essential that we relate how the parameters used in MGC techniques impact thin film formation and crystallization, as it will be instrumental in enhancing control over thin film formation and crystallization processes in multiple fields. During MGC, a solution/solute mixture is spread

as a thin layer upon a substrate, with coupled thermal control to achieve evaporative crystallization. A combination of meniscus geometry, thermal gradients, concentration gradients, and fluid flow contributes to directing thin film formation and crystallization in small molecules.[6] Recent studies in microfluidic systems have shown that fluid flow and shear can affect the final crystallization morphology.[14,15] Similar to microfluidic geometries, length scales on the order of microns are present during MGC film deposition, indicating that fluid flow and shear could also be highly relevant to crystallization and solid thin film formation, thus prompting study of the significance of coupled evaporation and fluid flow during MGC. Thus far, there is not a study that provides comprehensive molecular length scale understanding of the combined effects of fluid flow and evaporation on molecular assembly.[16,17]

It is assumed that the evaporation rate, coupled with fluid shear, influences the supersaturation and molecular orientations, which then impacts the crystallization behavior of the small molecules. However, the system is difficult to simulate with simple models, due to the simultaneous momentum, mass and thermal gradients, as well the solidification process of solute phase transformation into a solid (amorphous or crystalline thin film). Therefore, most of the understanding of small molecule flow coating processes comes from observation and formation of empirical relationships between processing conditions (temperature, concentration, deposition speed, etc.) and desired film characteristics. Le Berre et al. provided an empirical relationship combined with a system mass balance to explain the film thickness dependence on the coating conditions.[18] Empirical relationships between solvent boiling point and film quality were developed by Janneck et al.[19] Joshi et al. developed an analytical model to describe film drying and aggregation of colloids during a meniscus guided coating method.[20] These models help to inform experimental work, however, mechanistic understanding of how to fundamentally describe molecular assembly and crystallization in a flow coating process has not been developed.

Computational techniques can be utilized in conjunction with experiments to obtain a deeper understanding of how flow coating techniques form thin films of small molecules. Park et

al. used COMSOL Multiphysics (a partial differential equation solver) to describe meniscus guided printing in thin films of conjugated polymer materials.[21] While this work describes thin film formation, the modeling technique is limited in its ability to describe the molecular orientations within the resulting film. Mohommadi et al. used molecular dynamics (MD) simulation to describe polymer alignment in meniscus guided coating.[22] However, the behavior of a high molecular weight conjugated polymer differs from the behavior of a small molecule in solution and during solidification. In fact, polymers and other macromolecules are frequently added to solutions as flow stabilizers, explicitly because they impact the viscosity and flow profile of the solution.[23]

In this work, we develop a MD method to understand the molecular behavior of a simple small molecule, glycine, during a meniscus guided coating process. Thin films of glycine are fabricated experimentally using MGC, which are found to have varying degrees of crystal domain alignment, quantified using degree of polarization. A molecular dynamics simulation was developed to provide a platform for interpreting experimental observations at the molecular length scale. We produced a simulation set-up that can describe molecular aggregation during fluid evaporation and is capable of incorporating fluid flow effects. Further, after introducing a periodic shear at the fluid surface, we observed molecular aggregation and alignment that differs from the molecular assembly that occurs with evaporation alone. These results are consistent with experimental observations of what occurs during the MGC process. By changing the evaporation rate, we observe that molecular aggregation is sensitive to the rate of solvent removal. Moreover, the film deposition rate (as controlled by the coating speed) appears to have a significant impact on the alignment and orientation of glycine molecules in the final film. Developing a platform that can provide a molecular understanding of thin film assembly in coating processes will supplement our ability to design films with tunable properties. Working towards achieving a close match between experimental and computational results will allow us to design processes to control molecular assembly, and achieve a deeper understanding of thin film formation for multiple applications.

MATERIALS AND METHODS

Solution Shearing Thin Films

Glycine (98.5% purity, Sigma-Aldrich) solutions were prepared at a concentration of 10 mg mL^{-1} in ultrapure water. Solutions were filtered through a 0.2 µm syringe filter prior to use. Silicon wafers were cut into approximately 1 cm^2 pieces and were cleaned with toluene, acetone, water, and isopropyl alcohol. The substrates were dried with pressurized air to remove residual solvent and particulate matter on the surface. Wafers were then UV-ozone treated (Bioforce UV/Ozone ProCleaner Plus) for 10 minutes to create a sterile and hydrophilic surface. Through this, solvent surface wetting is enhanced and coffee ring effect is minimized.

An in-house built MGC equipment was used to fabricate the thin films. UV-ozone treated wafers were placed on a heated stage, set to a controlled temperature (T = 60 – 90 °C), with a vacuum applied to hold the substrate to the stage. A vacuum line fixed the coating blade above the wafer substrate. After pipetting a droplet (20 µL) of glycine solution between the substrate and coating blade, the blade was translated at specified speeds (0.3 – 1.3 mm s^{-1}) to create a thin layer of solution on the silicon substrate. As the solvent dried, a thin film of glycine was created on the substrate. Dropcast control samples were created through dropping 50 µL of glycine solution on a cleaned, and UV-ozone treated wafer.

Thin film characterization

After films were created, thickness was measured using a Zygo NewView 730 white light interferometer.[18] A Zeiss Axio Imager A.1 optical microscope with two polarizers oriented orthogonally produced linearly polarized light for characterizing thin film alignment and isotropy. Films were imaged using a Zeiss Axiocam 503 Color camera. The thin films were rotated incrementally under the cross polarizers to determine the relationship between sample orientation

and optical activity. This was quantified using the degree of polarization (DOP), which can describe alignment in a thin film.[24,25]

The degree of polarization is defined as:

$$DOP = \frac{I_{max} - I_{min}}{I_{max} + I_{min}}$$

where I_{max} is the maximum observed intensity and I_{min} is the minimum observed intensity of light that passes through the aligned film. The image intensity was quantified using the measure function in ImageJ, which provides an average pixel intensity count for the image to determine I_{min} and I_{max}. A DOP near 1 corresponds with an aligned thin film while a DOP closer to 0 indicates that the film is more isotropic.

Atomistic Modeling and Computational Method

The simulation was designed to match experimental conditions as closely as possible, with respect to understanding how fluid flow, shear, and solvent removal can impact the aggregation of glycine. All molecular dynamics simulations were performed with LAMMPS.[26] The timestep was set as 0.5 fs.

The solution consists of 812 molecules of glycine described by the AMBER potential which were evenly dispersed in 7920 molecules of water described by SPC/E model.[27–29] The initial location of the molecules was random to ensure that there was good mixing. The non-bonded van der Waals interactions between atoms were reproduced by the Lennard-Jones potential while the Coulomb interactions were calculated by PPPM method with a root mean of 0.0001.[30] The system contained 33,600 atoms in total, allowing for statistical conclusions to be drawn by looking at the average behavior of the ensemble.

Experimentally, the thin film is formed on top of a silicon wafer. A layer of silicon described by the Tersoff potential with the thickness of 1.6 nm and the lattice orientation of <1 0 0> was designated as the lower bound of the simulation box (at z = 0 nm).[31]

The size of the simulation box was set as 4.59 nm in x (length) direction, 4.78 nm in y (width) direction and 18.00 nm (thickness) direction, respectively. A Periodic boundary condition was applied in the length (x) and width (y) directions while a non-periodic boundary condition was applied in the thickness (z) direction.

Evaporation and solvent removal

Initially, the system was relaxed in canonical (NVT) ensemble for 2 ns to reach equilibrium at 383 K. Next, to simulate the evaporation process of the solvent water molecules, water molecules at the top surface of the solution were artificially removed from the system every 4 ps. The evaporation region thickness was determined as the van der Waals equilibrium distance between water molecules, namely 0.32 nm. Several evaporation rates of 1.25, 2.5, 3.75, and 15 molecules ps^{-1} were controlled by fixing the number of water molecules deleted at each time. The evaporation process took 2 - 7 ns. Similar simulation approaches are used to investigate the molecular morphology and self-assembly guided by rapid evaporation.[32,33]

Introducing fluid flow

During thin film coating, material is deposited on the substrate through horizontal translation of a coating blade across the surface. This was explored in the simulation by introducing a shear on the top surface of the molecules. In micro-canonical (NVE) ensemble, a constant speed in x-direction was exerted on the solution molecules at the top surface (air/liquid interface) across the periodic boundary. To ensure relaxation, the temperature was maintained at 383 K by rescaling the kinetic energy of the solution. After 1 ns, a stable velocity profile in x-z plane can be developed. Through this, the intent is to determine what impact the fluid flow has on molecular assembly in an evaporative environment. The flow velocity of 0, 200, 400, 600, and 800 m s^{-1} was chosen to match the Reynolds number in experimental setting with the Reynolds number in the simulation.

RESULTS AND DISCUSSION

Thin films were fabricated from aqueous glycine solutions using dropcasting and a MGC technique. Briefly, dropcasting produces a thin film by pipetting the aqueous glycine solution onto a silicon substrate with a controlled temperature, where evaporation results in the crystallization of glycine (**Figure 1a**). The films produced using dropcasting demonstrate isotropic crystal growth.

In MGC, as in dropcasting, evaporation is used to control crystallization. However, at the start of the process, a coating blade is held steady on top of the substrate (**Figure 1b**). After a droplet of the solution is placed on the substrate, capillary action pulls the liquid between the substrate and the blade, which is translated above along the substrate at a controlled speed. Evaporation and crystallization occur at the meniscus developed during this process, and produces a thin film. The controlled crystal growth of the sheared samples creates films with significantly different optical properties and surface morphology, compared to the samples created using dropcasting.

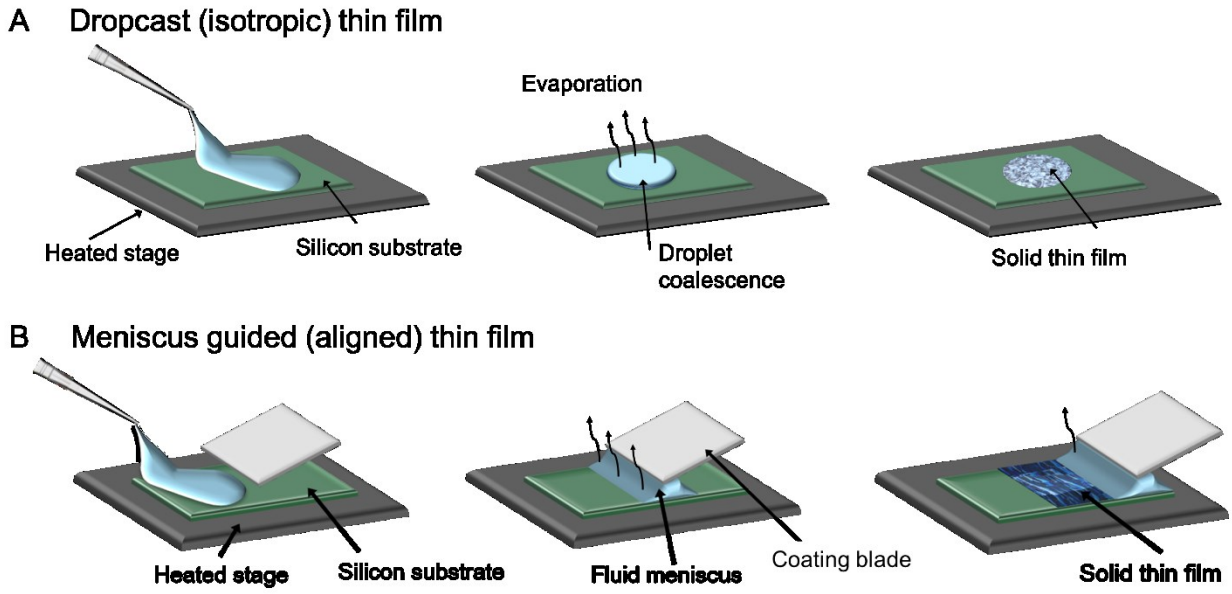

Figure 1: a) Dropcasting uses evaporation control to change the crystallization process, and creates films with isotropic morphology. b) Meniscus guided coating uses evaporation control and fluid flow to create a meniscus where coupled evaporation and flow occurs, resulting in crystallization with alignment of crystals in the thin film.

Dropcasting provides limited control over the crystallization process. From polarized optical microscopy (POM) images (**Figure 2a**), it is clear that as the temperature is increased, the size

of the individual crystal grains increases. We hypothesize that the change in grain size is related to the evaporation timescale, such that nucleation is dominant in the slow evaporation conditions while growth is favored in the fast evaporation condition (**SI Figure 1, 2**). Grain sizes for samples dropcasted at 60 and 70 °C were 194 ± 59 μm and 254 ± 65 μm respectively. The grain sizes were larger at higher dropcasting temperatures of 80, 90 and 100 °C, with the average measured sizes reaching 747 ± 334 μm, 622 ± 228 μm and 695 ± 334 μm (**SI Figure 2**). The optical

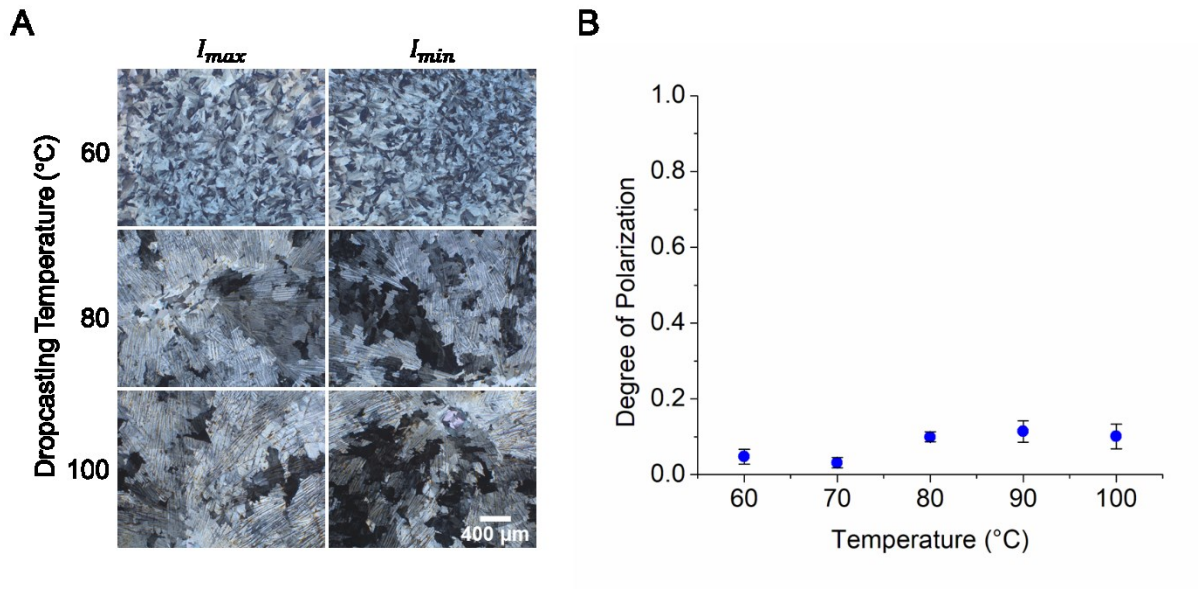

Figure 2: a) Polarized optical microscopy images of dropcast thin films at 60, 80, and 100 °C. As films are rotated under the polarizer, the orientations with maximum and minimum overall image intensity are shown. The scale bar is 400 μm for all images. b) The degree of polarization for dropcast films is low for all conditions, with higher temperatures having slightly higher DOP. The y-axis ranges from 0 - 1 to reflect the upper and lower bound of the DOP.

properties of the film were characterized using degree of polarization (DOP), defined in materials and methods and the SI. The DOP has a theoretical range of values between 0 (no alignment) and 1 (perfect alignment). The degree of polarization did not significantly change with processing temperature for dropcast samples (**Figure 2b**). We observe that the grain size of the crystals increases with increasing temperature, but that the thin film itself does not have a measurable change in the degree of polarization. Based on this, the dropcast films are characterized as isotropic across the length scale of the substrate and the evaporation rate is an important factor in changing grain size within the films.

MGC was then used to fabricate thin films, incorporating directed fluid flow in addition to evaporation. Coating speeds ranged from 0.3 – 1.3 mm s^{-1} with the substrate heated up to 90 °C. From previous studies, these conditions are ideal for creating smooth thin films.[8] The POM images demonstrate the drastic difference in grain size and alignment for the samples created using MGC (**Figure 3a**). For slow coating speeds, the crystal domains are wide and long; almost the entire film exhibits brightness at the same time (I_{max} is high) while in the whole film is dark (I_{min} is low) when the sample is rotated. As the coating speed increases to 0.7 mm s^{-1}, the domains become narrower and begin to show misalignment. For the fastest coating speed used in the study, 1.3 mm s^{-1}, the images show shorter and narrower domains in the coating direction, relative to the samples formed at a coating speed of 0.3 mm s^{-1}. For the fast coating condition, the film intensity of upon rotation is similar, indicating that I_{max} and I_{min} are converging to similar values, causing the DOP to approach 0 (**SI Figures 5, 6**). The films fabricated at slow coating speeds are composed of large domains compared to the films fabricated at faster speeds, which show more defects and smaller crystal domains. The presence of more defects at the faster coating speed is attributed to the increased nucleation in thinner films, breaking up otherwise coherent crystal domains.

DOP was quantified for solution sheared samples, created at 90°C (**Figure 3b**). We observe that when the processing speed is slow (0.3 mm s^{-1}), the thin film has a high DOP (0.57 ± 0.06) while the films created at faster speeds (1.3 mm s^{-1}) have a much lower degree of polarization (0.06 ± 0.02) similar to the values obtained for the dropcast samples created at 90 °C (0.11 ± 0.03).

In addition to optical characterization, grazing incidence X-ray diffraction (GIXD) was used to probe the crystal orientation and alignment in thin films (**SI Figure7**). GIXD corroborates the optical results, showing that meniscus guided coating creates conditions to produce aligned crystals: at slower coating speeds, films are more aligned compared to the faster coating condition.

Changing the coating speed controls the deposition of material from the meniscus, impacting the crystallization of glycine in the film. The experimental conditions utilized in this work provide reproducible film morphology and thickness (ranging from 30-120 nm, **SI Figure 4**) as a

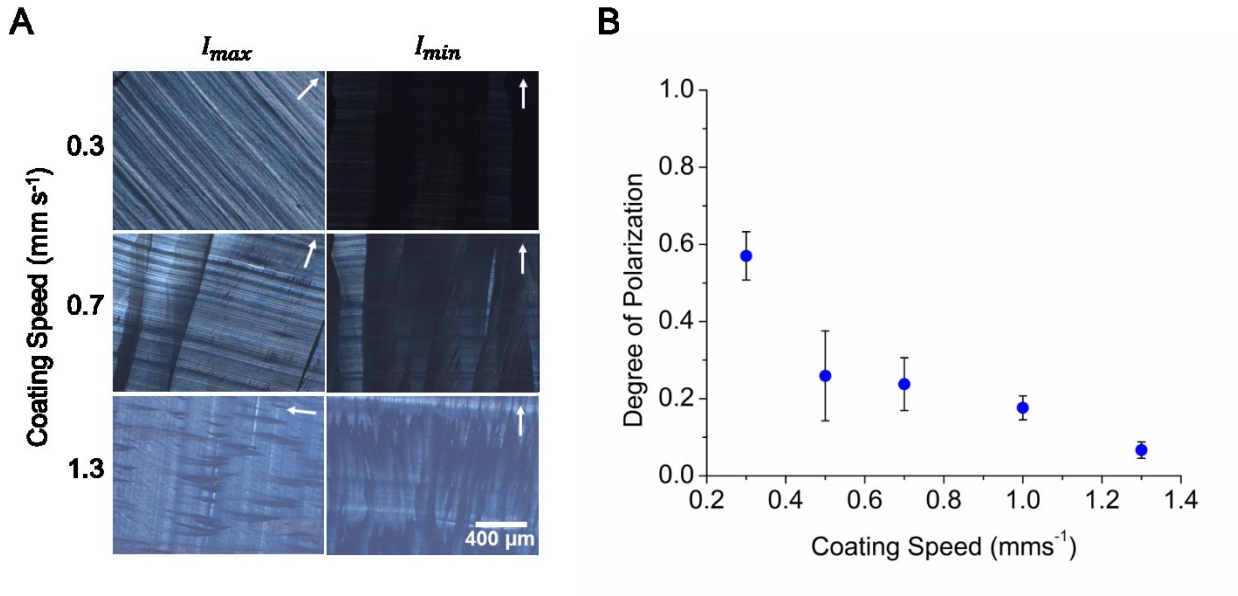

Figure 3 a) Polarized optical microscopy images of thin films created at 90 °C and 0.3, 0.7, and 1.3 mm s^{-1}. As the coating speed is increased, the films exhibit less redirection of the cross-polarized incident light. The slow coating speed produces films where I_{max} and I_{min} are drastically different. Scale bar is 400 µm and is the same for each image. Arrows demonstrate the shearing direction. b) The degree of polarization shows a dependence on shearing speed, with fast coating speeds having lower DOP.

function of coating speed, indicating film growth was in the evaporative regime (**SI Figure 3, SI Figure 4**).[18] In the evaporative regime of MGC, the evaporation timescale and thin film deposition (and crystallization) timescales are similar, facilitating aligned crystal growth.

Experimental work alone is limited in the ability to draw detailed conclusions about how molecules crystallize in an aligned manner during flow coating. Manipulating a processing condition (e.g. coating speed) and characterizing film response (e.g. degree of polarization) is an inefficient process. Therefore, there is a motivation to understand how flow parameters and flow profiles facilitate molecular alignment. Developing a platform that provides molecular insight to thin film assembly processes with coupled evaporation and flow fields can supplement our understanding of complex coating processes, at length scales not accessible by experimental approaches.

Differences between dropcast crystallization and MGC based crystallization were used to inform the design of a model where molecular dynamics can help clarify how molecular aggregation and assembly occurs in response to evaporation and fluid shear. Experimental results showed that the incorporation of flow with evaporation improves thin film alignment. Therefore, we hypothesize that matching the approximate Reynolds number (Re) when translating experimental work is necessary (Supplementary Information) to capture the importance of fluid mechanics that occur in a coating process. The aim of developing a molecular dynamics model is to gain understanding of the mechanisms of alignment in response to shear flow profiles.

Evaporation of the solvent (water) was modeled using a molecular dynamics approach. The region of interest was chosen as the region where crystallization is actively occurring in experiments (**Figure 4**). This was translated to a model where a silicon substrate bounds the lower z-axis, and a glycine/water mixture was layered on top of the substrate. Finally, solvent removal was restricted to occur at the top surface, in order to better model the evaporation process (**Figure 4a**). Solvent molecules were allowed to exit the system at specified rates, in order to model a constant evaporation rate.

A snapshot of the evaporation process shows that the initially well-dispersed system (t = 0 ns) transforms to a glycine only system after 6.55 ns (**Figure 4 b,c**). The intermediate timepoints demonstrate enrichment of glycine molecules at the top interface. Plotting the density profile as a function of distance from the substrate, it is clear that removing solvent from the top surface results in aggregation and densification of the glycine molecules at the interface (**Figure 4c**). Similar phenomena were observed at different evaporation rates (**SI Figure 8**). This result mirrors the experimental formation of thin films, where it is commonly observed that solidification occurs at the air-liquid interface.[34,35]

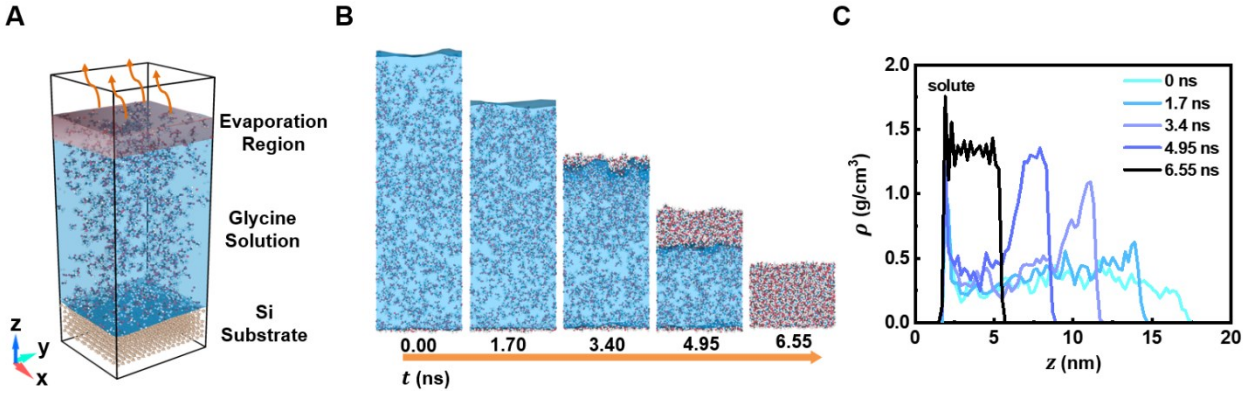

Figure 4: a) Evaporation was developed in simulation with a water/glycine solution with water exiting the system from the top boundary of the simulation box. b) During simulation progression, water molecules are removed from the system, resulting in preferential aggregation of glycine at the top surface. c) The simulation produces a densified, solid glycine film.

After the solvent molecules were completely removed, the orientation of the glycine molecules remaining in the system is stable, which is indicated by the evolution of the potential energy of the system and a density profile that does not change with time (**SI Figure 9**). In glycine, unique bonding motifs can be used to track molecular orientation. The carbon-carbon (C-C) bond is unique and can be used to identify a statistical distribution of the direction that the glycine molecules are pointing. Therefore, for each glycine molecule, the angles between the direction of the C-C bond (schematic in **Figure 5a**) and coordinate axes (θ_{x-CC}, θ_{y-CC}, and θ_{z-CC}) after

evaporation were recorded and plotted on a surface, with the z-direction pointing normal to the substrate (x-y) plane.

We observe that fast removal of solvent from the system results in less order relative to slow removal of solvent. In **Figure 5b**, the slowest evaporation case shows several "hot spots" where many glycine molecules preferentially are aligned with the C-C bonding axis pointing in a direction perpendicular to the substrate (i.e., z-direction, $\cos(\theta_z - CC)$ =0). The P heatmap denotes the probability density, and is calculated by the number of glycine molecules with a specific pointing direction normalized by the total number of glycine molecules. In other words, the value at the surface for P sums as unity.

These results show that as solvent removal rate is decreased, glycine molecules are more oriented. For the fast evaporation condition (15 molecules ps^{-1}), the resulting glycine film is more

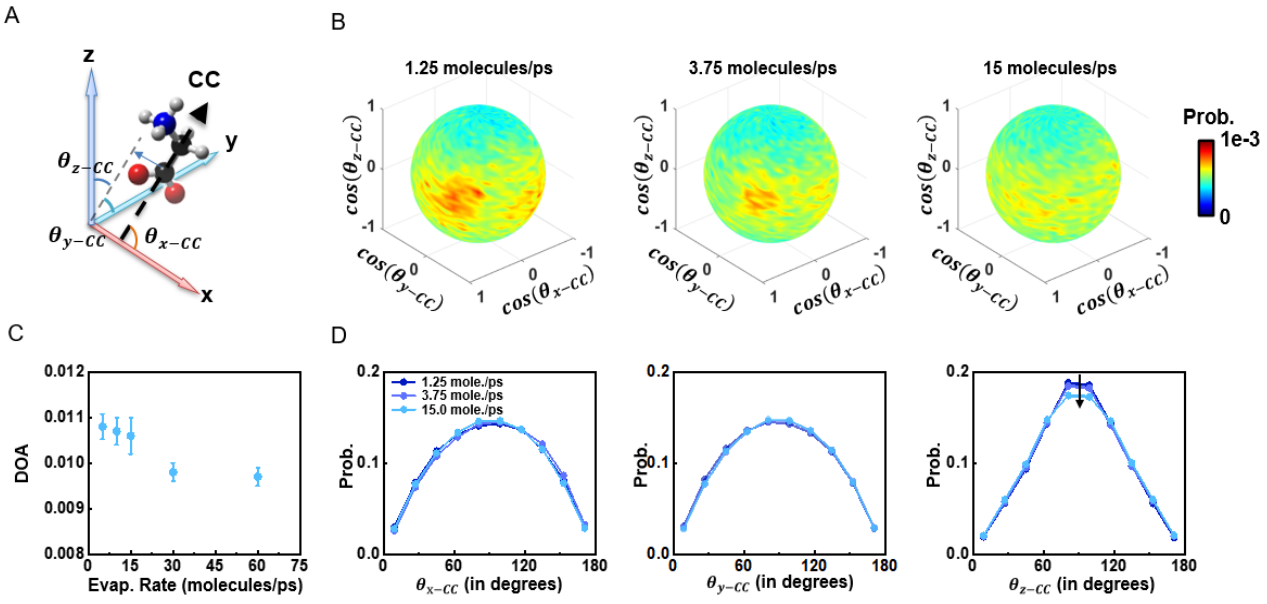

Figure 5: a) Schematic of the orientation characterization. b) Changing evaporation rate during simulation was used to determine the ideal condition for observing glycine aggregation and the extent of orientation in the final film. The C-C bond orientation in glycine is shown by the orange arrow in the glycine molecule. Slow evaporation (1.25 molecules ps^{-1}) produced more ordered glycine during simulation. c) Degree of Alignment (DOA) decreases with the evaporation rates. d) Same information can be reflected by the glycine molecule orientations collapsed to x, y and z directions at different evaporation rates.

disordered, indicated by the lowered probability of alignment across the surface for faster

evaporation rates in $(\theta_z - CC)$ (**Figure 5b**). However, when the evaporation rate is slowed down to (1.25 molecules ps^{-1}) the glycine molecules begin to exhibit an ability to orient along the z-axis (**Figure 5b**). The spatial characterization of the C-C bond orientation suggests these orientations along z-axis result from the interaction between the substrate and glycine molecules (**SI Figure 10**). To quantitatively describe the alignment of the glycine molecules from their orientations and compare with the DOP from experiments we define the degree of alignment (DOA) as $DOA = \frac{N_{ori}}{N}$, where N_{ori} and N respectively denote the number of C-C bonds oriented in the most popular direction, and the total number of glycine molecules. The direction has a tolerance of 18^o, leading to $N_{dir} = \left(\frac{360^o}{tolerance}\right)^2 = 400$ directions to be considered in calculations. A DOA near 1 corresponds with perfect molecular alignment while a low DOA approaching $\frac{1}{N_{dir}} = 0.0025$ indicates isotropic molecular orientations, as with the DOP measurement. This provides similar measures for comparison of trends between experiment and simulation.

Figure 5c shows that a higher evaporation rate suppresses the DOA slightly, which is consistent with the orientation distribution as seen in **Figure 5b**. To further elaborate the change in the orientations of the glycine molecules due to the variation in evaporation rate, we project the 3D orientations into 1D orientations, namely the angle between the C-C bond in each glycine molecule and the x, y and z-axes (**Figure 5d)**. Increasing the evaporation rate decreases the orientation of glycine molecules in z-direction, as marked by the black arrow. However, from the experimental dropcast DOP study (**Figure 2**), we observe that there is only a small change in the effective order in the thin film MGC (**Figure 3)**. We hypothesize that the alignment observed in the MD simulations are analogous to local ordering, which are not observable in the large-scale domains studied using optical microscopy.

Since crystallization is a process that requires both densification and long-range order of molecules, the slow evaporation simulation is the best approximation of an evaporation based molecular aggregation, as fast evaporation simulations do not achieve a high degree of order.

The goal is to develop a simulation that can demonstrate the ability of the fluid flow to orient molecules alongside the evaporative process of creating an ordered solid. Therefore, we chose to proceed with simulating the effects of fluid flow using the slow evaporation condition (1.25 molecules ps^{-1} removed). Meniscus guided coating techniques, such as MGC, rely on capillary forces to create a meniscus between the substrate and the coating blade. The fluid in contact with the top blade moves at the same speed as the blade while the fluid at the substrate can be approximated as having a no-slip condition, and is stationary.[36] Since crystallization proceeds at the air-liquid interface where the solvent molecules are leaving the system, the region of interest remains the same as the evaporation only simulation.

Figure 6a demonstrates the stable velocity profile along z-direction when a flow at different velocities is applied at the top surface of the simulation box. **Figure 6b** shows several snapshots in the presence of the velocity profile. Visually, both the water and glycine molecules initially on the left side of the simulation box are tagged as black and snapshots of the simulation show the evolution of the flow profile. Driven by the shear flow, after 10 ps, the marked particles in the top layer has traveled a full period of the box in x-direction, entering the system from the other side, while the particles closer to the substrate has traveled a limited distance due to the non-slip layer attached to the substrate. Consequently, the marked profile is extended by multiple periods in x-direction. Water (solvent) molecules were removed from the simulation at a rate of 1.25 molecules ps^{-1} with the periodic shear present in the system.

After all solvent molecules were removed, the C-C bond direction of the glycine molecules was characterized to study the alignment of the solid thin film (**Figure 7**). The direction of the shear flow is marked by the arrows in the schematic in **Figure 7a**. As shear is introduced, we observe that the direction of the glycine molecule alignment changes, as seen by the shift in the position of the hot spot on the orientation map (**Figure 7b**). We attribute this molecular reorientation as a response to the flow profile introduced in the simulation. For the fast flow case

(400 m s^{-1}) we observe that the hot spot matches the flow direction, namely the positive x-direction.

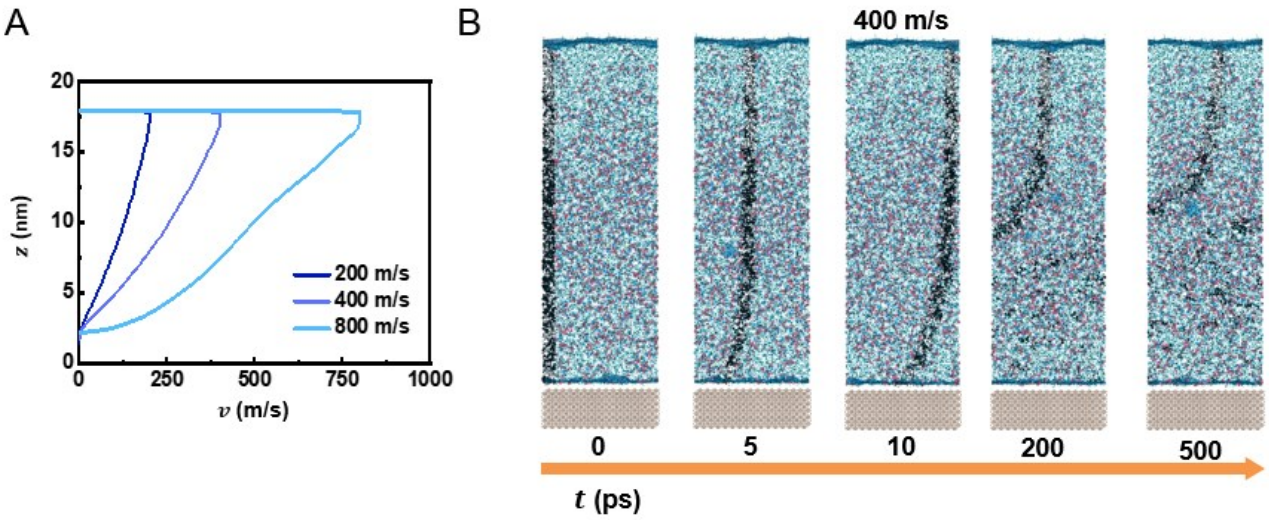

Figure 6: a) Velocity profile along z-direction in the presence of a flow applied at the top interface. b) Snapshots at different moments when the flow at the top interface is at 400 m s^{-1}.

The change of the alignment orientation can also be reflected by monitoring the DOA in two specific orientations (**Figure 7c**), namely the alignment orientation in the absence of shear flow orientation 1 ($\theta_{x-CC} = 0$, $\theta_{y-CC} = 90^o$ and $\theta_{z-CC} = 90^o$) and in the presence of a shear flow with high velocity 400 m/s , termed orientation 2 ($\theta_{x-CC} = 90$, θ_{y-CC} and $\theta_{z-CC} = 0^o$)), as marked in **Figure 7b.** The increasing and decreasing DOAs at a faster speed in orientation 1 and 2 demonstrate the change of the orientation of the glycine molecules. Moreover, in **Figure 7d**, the shear flow in x-direction (i.e., $\theta_{x-CC} = 0$, θ_{y-CC} and $\theta_{z-CC} = 90^o$) leads to the alignment of the C-C bond in the direction of the flow. At a higher evaporation rate, a higher velocity is needed to change the orientation of the C-C bonds to align with the flow direction (**SI Figure 11**). Therefore, we see that the evaporation and fluid flow can both introduce alignment within the solid thin film.

The simulation work demonstrates that when an evaporative process exists in the presence of continuous shear velocity, glycine molecules in the velocity field are able to orient and respond to the flow. This is reflected in the experimental work through the alignment of

crystalline domains in the direction of shearing as well, characterized by the degree of polarization.

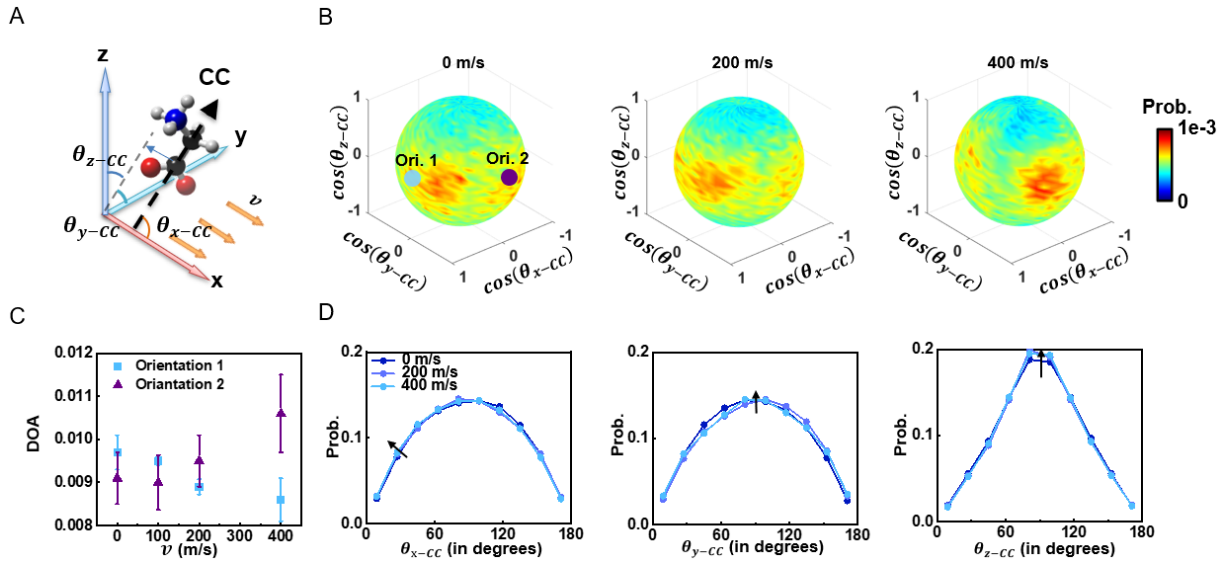

Figure 7: In the presence of a continuous flow profile, after solvent removal is complete, the orientation of glycine molecules is plotted. For all cases, water molecules are removed at a rate of 1.25 molecules ps^{-1}. a) schematic of the orientation characterization in the presence of a shear flow. In b), carbon-carbon bond direction for all glycine molecules is displayed, with simulated coating speeds of 0, 200 and 400 m s^{-1}. c) Higher velocity of the shear flow forces the shift of the alignment orientation. d) 1D orientations of the glycine molecules at different shearing flow velocities.

CONCLUSIONS

In this work, the ability to create aligned thin films of glycine using MGC was demonstrated. We found that MGC improves the ordering of molecules to create aligned crystalline domains. The degree of alignment was characterized using the DOP, which showed that films created at slow coating speeds exhibit more alignment relative to the films created at faster coating speeds. The observed experimental trends are likely generalizable across many molecular systems, and are consistent with previously reported results regarding tunable alignment obtained using thin film coating platforms.[37,38] Further, the DOP characterization technique is widely applicable to characterize the degree of alignment or isotropy within a thin film sample. The experimental

results were used to design a molecular dynamics simulation to model the evaporation and the fluid flow that occurs during MGC.

From the simulation, we observed that changing the evaporation rate can produce different molecular aggregation trends. Fast evaporation resulted in a highly random arrangement of glycine molecules while slowing the evaporation down facilitated molecular aggregation in the x-y plane of the substrate. This corroborates experimental results, where evaporation rate was significant in changing observable grain size of dropcast thin films. This suggests that the evaporation rate is significant in producing order during thin film crystallization.

Next, a flow profile was introduced to the simulation to understand how MGC is able to contribute to molecular alignment and the formation of aligned domains. The DOA parameter was used to characterize the molecular orientation of glycine, showing that changing the coating speed changes the preferred directionality of the ensemble of glycine molecules. This observation holds true across experimental and simulation. This suggests that the flow is able to influence the motion of glycine in solution and that after evaporation, the thin film exhibits order that is dependent on the flow profile.

Multiple experimental works report that molecular alignment is sensitive to evaporation and fluid flow. We are only just beginning to use sophisticated simulations to understand the underlying phenomena that facilitate the observed alignment. This work presents the foundations of bridging experimental observations with a tangible understanding of molecular-level ordering that occurs in MCG processes. Future work will be focused on understanding and modeling phase transformations that occur in glycine and other organic molecules during MGC. Because modeling can provide transient descriptions of film formation, modeling can be coupled with existing techniques, such as in situ grazing incidence x-ray diffraction and in situ optical microscopy and spectroscopy for enhanced mechanistic understanding.[39–41]

SUPPORTING INFORMATION

Supporting information further describes thin film characterization, degree of polarization measurements. developing and validating the molecular dynamics simulation.

ACKNOWLEDGEMENTS

B. X. acknowledges the funding support from NSF-CBET-1805451. Y.G. would like to acknowledge the support from the John Bell McGaughy Fellowship at the University of Virginia. G.G. acknowledges support from the Jefferson Trust and the UVA Research Innovation Award. G.G. and S.G. acknowledge funding support from the Thomas F. and Kate Miller Jeffress Memorial Trust.

WORKS CITED

(1) Kirwan, D. J.; Orella, C. J. Crystallization in the Pharmaceutical and Bioprocessing Industries. In *Handbook of Industrial Crystallization*; Myerson, A. S., Ed.; Elsevier Inc., 2002; pp 249–266.

(2) Hartel, R. W. Crystallization in Foods. In *Handbook of Industrial Crystallization*; Meyerson, A. S., Ed.; Elsevier Inc., 2002; pp 287–304.

(3) Qu, G.; Kwok, J. J.; Diao, Y. Flow-Directed Crystallization for Printed Electronics. *Acc. Chem. Res.* **2016**, *49* (12), 2756–2764.

(4) Tsarfati, Y.; Rosenne, S.; Weissman, H.; Shimon, L. J. W.; Gur, D.; Palmer, B. A.; Rybtchinski, B. Crystallization of Organic Molecules: Nonclassical Mechanism Revealed by Direct Imaging. *ACS Cent. Sci.* **2018**, *4* (8), 1031–1036.

(5) Jain, M.; Lohare, G.; Bari, M.; Chavan, R.; Barhate, S.; Shah, C. Spray Drying in Pharmaceutical Industry: A Review. *Res. J. Pharm. Dos. Forms Technol.* **2012**, *4* (2), 74–79.

(6) Coliaie, P.; Kelkar, M. S.; Nere, N. K.; Singh, M. R. Continuous-Flow, Well-Mixed, Microfluidic Crystallization Device for Screening of Polymorphs, Morphology, and Crystallization Kinetics at Controlled Supersaturation. *Lab Chip* **2019**, *19*, 2373–2382.

(7) Thabet, Y.; Sibanc, R.; Breitkreutz, J. Printing Pharmaceuticals by Inkjet Technology: Proof of Concept for Stand-Alone and Continuous in-Line Printing on Orodispersible Films. *J. Manuf. Process.* **2018**, *35*, 205–215.

(8) Guthrie, S. M.; Smilgies, D. M.; Giri, G. Controlling Polymorphism in Pharmaceutical Compounds Using Solution Shearing. *Cryst. Growth Des.* **2018**, *18* (2), 602–606.

(9) Horstman, E. M.; Kafle, P.; Zhang, F.; Zhang, Y.; Kenis, P. J. A. A.; Diao, Y. Solution Coating of Pharmaceutical Nanothin Films and Multilayer Nanocomposites with Controlled Morphology and Polymorphism. *ACS Appl. Mater. Interfaces* **2018**, *10* (12), 10480–10489.

(10) Giri, G.; Delongchamp, D. M.; Reinspach, J.; Fischer, D. A.; Richter, L. J.; Xu, J.; Benight, S.; Ayzner, A.; He, M.; Fang, L.; Xue, G.; Toney, M. F.; Bao, Z. Effect of Solution

Shearing Method on Packing and Disorder of Organic Semiconductor Polymers. *Chem. Mater.* **2015**, *27* (7), 2350–2359.

(11) Diao, Y.; Tee, B. C. K.; Giri, G.; Xu, J.; Kim, D. H.; Becerril, H. A.; Stoltenberg, R. M.; Lee, T. H.; Xue, G.; Mannsfeld, S. C. B.; Bao, Z. Solution Coating of Large-Area Organic Semiconductor Thin Films with Aligned Single-Crystalline Domains. *Nat. Mater.* **2013**, *12* (7), 665–671.

(12) He, Z.; Chen, J.; Li, D. Review Article: Crystal Alignment for High Performance Organic Electronics Devices. *J. Vac. Sci. Technol. A* **2019**, *37* (4), 40801.

(13) Nagar, P.; Singh, K.; Chauhan, I.; Verma, M.; Yasir, M.; Khan, A.; Sharma, R.; Gupta, N. Orally Disintegrating Tablets : Formulation, Preparation Techniques and Evaluation. *J. Appl. Pharm. Sci.* **2011**, *1* (4), 35–45.

(14) Giri, G.; Yang, L.; Mo, Y.; Jensen, K. F. Adding Crystals to Minimize Clogging in Continuous Flow Synthesis. *Cryst. Growth Des.* **2019**, *19* (1), 98–105.

(15) Stroobants, S.; Callewaert, M.; Krzek, M.; Chinnu, S.; Gelin, P.; Ziemecka, I.; Lutsko, J. F.; De Malsche, W.; Maes, D. Influence of Shear on Protein Crystallization under Constant Shear Conditions. *Cryst. Growth Des.* **2020**, *20* (3), 1876–1883.

(16) Lee, T.; Sanzogni, A. V.; Burn, P. L.; Mark, A. E. Evolution and Morphology of Thin Films Formed by Solvent Evaporation: An Organic Semiconductor Case Study. *ACS Appl. Mater. Interfaces* **2020**, *12* (36), 40548–40557.

(17) Gertsen, A. S.; Sørensen, M. K.; Andreasen, J. W. Nanostructure of Organic Semiconductor Thin Films: Molecular Dynamics Modeling with Solvent Evaporation. *Phys. Rev. Mater.* **2020**, *4*, 075405.

(18) Le Berre, M.; Chen, Y.; Baigl, D. From Convective Assembly to Landau - Levich Deposition of Multilayered Phospholipid Films of Controlled Thickness. *Langmuir* **2009**, *25* (5), 2554–2557.

(19) Janneck, R.; Vercesi, F.; Heremans, P.; Genoe, J.; Rolin, C. Predictive Model for the Meniscus-Guided Coating of High-Quality Organic Single-Crystalline Thin Films. *Adv. Mater.* **2016**, *28* (36), 8007–8013.

(20) Joshi, K.; Gilchrist, J. F. Estimation of Drying Length during Particle Assembly by Convective Deposition. *J. Colloid Interface Sci.* **2017**, *496*, 222–227.

(21) Park, K. S.; Kwok, J. J.; Dilmurat, R.; Qu, G.; Kafle, P.; Luo, X.; Jung, S. H.; Olivier, Y.; Lee, J. K.; Mei, J.; Beljonne, D.; Diao, Y. Tuning Conformation, Assembly, and Charge Transport Properties of Conjugated Polymers by Printing Flow. *Sci. Adv.* **2019**, *5* (8), eaaw7757.

(22) Mohammadi, E.; Zhao, C.; Meng, Y.; Qu, G.; Zhang, F.; Zhao, X.; Mei, J.; Zuo, J. M.; Shukla, D.; Diao, Y. Dynamic-Template-Directed Multiscale Assembly for Large-Area Coating of Highly-Aligned Conjugated Polymer Thin Films. *Nat. Commun.* **2017**, No. 8, 16070.

(23) Dinic, J.; Sharma, V. Macromolecular Relaxation, Strain, and Extensibility Determine Elastocapillary Thinning and Extensional Viscosity of Polymer Solutions. *Proc. Natl. Acad. Sci. U. S. A.* **2019**, *116* (18), 8766–8774.

(24) Ye, L.; Li, F.; Lu, C.; Cheng, Z.; Hu, G.; Lu, Y.; Cui, Y. The Controllable Intensity and

Polarization Degree of Random Laser from Sheared Dye-Doped Polymer-Dispersed Liquid Crystal. *Nanophotonics* **2017**, *7* (2), 473–478.

(25) Bi, Z. F.; Yang, M.; Shang, G. Y. Optical Polarization Response at Gold Nanosheet Edges Probed by Scanning Near-Field Optical Microscopy. *Chinese Phys. B* **2018**, *27* (8), 087801.

(26) Plimpton, S. Fast Parallel Algorithms for Short-Range Molecular Dynamics. *J. Comput. Phys.* **1995**, *117* (1), 1–19.

(27) Duan, Y.; Wu, C.; Chowdhury, S.; Lee, M. C.; Xiong, G.; Zhang, W.; Yang, R.; Cieplak, P.; Luo, R.; Lee, T.; Caldwell, J.; Wang, J.; Kollman, P. A Point-Charge Force Field for Molecular Mechanics Simulations of Proteins Based on Condensed-Phase Quantum Mechanical Calculations. *J. Comput. Chem.* **2003**, *24* (16), 1999–2012.

(28) Cornell, W. D.; Cieplak, P.; Bayly, C. I.; Gould, I. R.; Merz, K. M.; Ferguson, D. M.; Spellmeyer, D. C.; Fox, T.; Caldwell, J. W.; Kollman, P. A. A Second Generation Force Field for the Simulation of Proteins, Nucleic Acids, and Organic Molecules. *J. Am. Chem. Soc.* **1995**, *117* (19), 5179–5197.

(29) Berendsen, H. J. C.; Grigera, J. R.; Straatsma, T. P. The Missing Term in Effective Pair Potentials. *J. Phys. Chem.* **1987**, *91* (24), 6269–6271.

(30) Zhang, J.; Hong, Y.; Liu, M.; Yue, Y.; Xiong, Q.; Lorenzini, G. Molecular Dynamics Simulation of the Interfacial Thermal Resistance between Phosphorene and Silicon Substrate. *Int. J. Heat Mass Transf.* **2017**, *104*, 871–877.

(31) Tersoff, J. New Empirical Approach for the Structure and Energy of Covalent Systems. *Phys. Rev. B* **1988**, *37* (12), 6991–7000.

(32) Liu, Q.; Xu, B. Liquid-Evaporation-Assisted Self-Folding of One-Dimensional Nanomaterials. *J. Phys. Chem. C* **2018**, *122* (5), 3078–3090.

(33) Liu, Q.; Gao, Y.; Xu, B. Liquid Evaporation-Driven Folding of Graphene Sheets. *Appl. Phys. Lett.* **2016**, *108*, 141906.

(34) Chen, A. Z.; Shiu, M.; Ma, J. H.; Alpert, M. R.; Zhang, D.; Foley, B. J.; Smilgies, D. M.; Lee, S. H.; Choi, J. J. Origin of Vertical Orientation in Two-Dimensional Metal Halide Perovskites and Its Effect on Photovoltaic Performance. *Nat. Commun.* **2018**, *9* (1), 1–7.

(35) Riera-Galindo, S.; Tamayo, A.; Mas-Torrent, M. Role of Polymorphism and Thin-Film Morphology in Organic Semiconductors Processed by Solution Shearing. *ACS Omega* **2018**, *3* (2), 2329–2339.

(36) Day, M. A. The No-Slip Condition of Fluid Dynamics. *Erkenntnis* **1990**, *33*, 285–296.

(37) Giri, G.; Verploegen, E.; Mannsfeld, S. C.; Atahan-Evrenk, S.; Kim do, H.; Lee, S. Y.; Becerril, H. A.; Aspuru-Guzik, A.; Toney, M. F.; Bao, Z. Tuning Charge Transport in Solution-Sheared Organic Semiconductors Using Lattice Strain. *Nature* **2011**, *480* (7378), 504.

(38) Sanchez-Botero, L.; Dimov, A. V.; Li, R.; Smilgies, D. M.; Hinestroza, J. P. In Situ and Real-Time Studies, via Synchrotron X-Ray Scattering, of the Orientational Order of Cellulose Nanocrystals during Solution Shearing. *Langmuir* **2018**, *34* (18), 5263–5272.

(39) Smilgies, D. M.; Li, R.; Giri, G.; Chou, K. W.; Diao, Y.; Bao, Z.; Amassian, A. Look Fast:

Crystallization of Conjugated Molecules during Solution Shearing Probed in-Situ and in Real Time by X-Ray Scattering. *Phys. Status Solidi - Rapid Res. Lett.* **2013**, *7* (3), 177–179.

(40) Gu, X.; Gunkel, I.; Hexemer, A.; Gu, W.; Russell, T. P. An in Situ Grazing Incidence X-Ray Scattering Study of Block Copolymer Thin Films during Solvent Vapor Annealing. *Adv. Mater.* **2014**, *26* (2), 273–281.

(41) Li, Y.; Wan, J.; Smilgies, D. M.; Bouffard, N.; Sun, R.; Headrick, R. L. Nucleation and Strain-Stabilization during Organic Semiconductor Thin Film Deposition. *Sci. Rep.* **2016**, *6*, 32620.